



## ORIGINAL ARTICLE

# Comparison of the rate constants of a bimolecular reaction using two methods



F. Shojaie

International Center for Science, High Technology & Environmental Sciences, Kerman, Iran

Received 5 February 2012; accepted 17 July 2012

Available online 4 August 2012

## KEYWORDS

Rate constant;  
RRKM;  
Vibrational mode analysis

**Abstract** There are different methods to calculate the rate constant of a bimolecular reaction. In this article are described two methods to calculate the rate constant and then these methods are compared using two-channel reaction. The rate constants for each reaction channel are calculated using Transition State Theory (TST) incorporating the Winger tunneling correction and the hindered rotor approximation. Furthermore, the rate constants for the dominant channel are calculated using general equation, which takes into account the rotational energy, is derived from Rice–Ramsperger–Kassel–Marcus (RRKM) theory, using the simplified version of the statistical adiabatic channel model theory. The vibrational mode analysis is used to elucidate the relationships of the reactant region ( $s = -\infty$ ), the saddle point ( $s = 0$ ) and the product region ( $s = +\infty$ ).

© 2012 Production and hosting by Elsevier B.V. on behalf of King Saud University. This is an open access article under the CC BY-NC-ND license (<http://creativecommons.org/licenses/by-nc-nd/3.0/>).

## 1. Introduction

The aim of this article is a comparison between the results of the rate constants that are calculated using Transition State Theory and general equations are derived on the basis of RRKM theory (Kenneth et al., 1996) which was adapted by Jerzy et al. (1998a,b, 1999) using the statistical adiabatic channel model (SSAM) (Jurgen, 1986) and specifically the simplified version (SSACM) developed by Jurgen, 1983; Cobos et al., 1985). At first, two methods for calculation of the rate constant are described, and consequently, these methods are

used for a two-channel reaction. The obtained results are compared with together as well as the existing experimental data.

The mechanism of a bimolecular reaction can be described as a two-step mechanism:



$k_a$  and  $k_{-a}$  are the forward and reverse rate constants for the first step,  $k_b$  corresponds to the second step. Based on the steady state analysis, the total rate constant can be written as:

$$k = \frac{k_a k_b}{k_{-a} + k_b} \quad (3)$$

As discussed in the papers of Annia et al. (2002, 2004),  $k_{-a}$  is considered to be much larger than  $k_b$ , so the above  $k$  can be written as:

$$k = \frac{k_a k_b}{k_{-a}} = K_{eq} k_b \quad (4)$$

E-mail address: fahimeh\_shojaie@yahoo.com

Peer review under responsibility of King Saud University.



Production and hosting by Elsevier

<http://dx.doi.org/10.1016/j.arabjc.2012.07.016>

1878-5352 © 2012 Production and hosting by Elsevier B.V. on behalf of King Saud University.

This is an open access article under the CC BY-NC-ND license (<http://creativecommons.org/licenses/by-nc-nd/3.0/>).

where  $K_{\text{eq}}$  is the equilibrium constant between the isolated reactants and the reactant complex. Applying basic statistical thermodynamic principles,  $K_{\text{eq}}$  can be expressed as:

$$K_{\text{eq}} = \frac{Q_{\text{RC}}}{Q_{\text{R}}} \exp \left[ \frac{E_{\text{R}} - E_{\text{RC}}}{RT} \right] \quad (5)$$

where  $Q_{\text{RC}}$  and  $Q_{\text{R}}$  are partition functions corresponding to the reactant complex and the isolated reactants, respectively. Under higher-pressure limit, in a unimolecular process, an equilibrium distribution of reactants is maintained, and the TST approach can be applied to calculate  $k_{\text{b}}$  (the second step), as:

$$k_{\text{b}} = \kappa \frac{k_{\text{B}}T}{h} \frac{Q_{\text{TS}}}{Q_{\text{RC}}} \exp \left[ \frac{E_{\text{RC}} - E_{\text{TS}}}{RT} \right] \quad (6)$$

where  $\kappa$  is the tunneling factor,  $k_{\text{B}}$  and  $h$  are the Boltzmann and Planck constants, respectively, and  $Q_{\text{TS}}$  is the transition state partition function. Thus, the effected rate constant is obtained as:

$$k = k_{\text{eq}}k_{\text{b}} = \kappa \frac{k_{\text{B}}T}{h} \frac{Q_{\text{TS}}}{Q_{\text{R}}} \exp \left[ \frac{E_{\text{R}} - E_{\text{TS}}}{RT} \right] \quad (7)$$

So the rate constant corresponding to all the studied reaction channels can be analyzed in terms of TST, a similar case has been found for the reactions of several volatile organic compounds with OH radical (Juan-Raúl et al., 2001, 2004; Victor et al., 2006).

In addition, the mechanism of a bimolecular reaction can be processed with the following pathway:



Bimolecular reactions, which involve the formation of intermediate molecular complexes often show unusual temperature and pressure dependence (Jurgen, 1994). In the case of loosely bound intermediates their collisional stabilization can, in first approximation, be omitted in description of the reaction rate. A method for rate constant calculation for a bimolecular reaction, which proceeds through formation of two intermediates complexes, has been proposed and successfully applied to describe the kinetics of the H-abstraction from methanol (Jerzy et al., 1998a). General equation, which takes into account the rotational energy, is derived from RRKM theory. According to this formalism, the rate constant for mechanism of (8) can be expressed:

$$k_{\text{obs}} = \frac{z}{hQ_{\text{A}}Q_{\text{B}}} \int_{V_{\text{TS}}}^{\infty} \sum_J W_{\text{F}}(E, J) \frac{W_{\text{TS}}(E, J)}{W_{\text{F}}(E, J) + W_{\text{TS}}(E, J)} \times \frac{W_{\text{G}}(E, J)}{W_{\text{G}}(E, J) + W_{\text{TS}}(E, J)} e^{-E/RT} dE \quad (9)$$

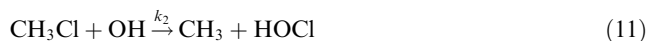
where  $Q_{\text{A}}$  and  $Q_{\text{B}}$  are the partition functions of A and B, respectively, with the center of mass translational partition function factored out of the product  $Q_{\text{A}}Q_{\text{B}}$ , and included in  $z$  together with the partition functions of those inactive degree of freedom which are not considered by the sums of the states under the integral.  $V_{\text{TS}}$  is the threshold energy toward the reactants A + B whereas  $W_{\text{TS}}(E, J)$ ,  $W_{\text{F}}(E, J)$  and  $W_{\text{G}}(E, J)$  denote the sum of the states at energy less than or equal to  $E$ , and the angular momentum  $J$  for the transition state TS and the activated complexes for the unimolecular dissociations of F and G, respectively. All computational effort is then related to the calculation of the sum of states,  $W(E, J)$ . This calculation

depends on the level at which the angular momentum conservation is considered, and it is discussed in detail in Jerzy et al. (1998a).

Now, these methods are described with two-channel reaction and then the results have been compared with available experimental data.

## 2. Computation method

The mechanism and kinetic of  $\text{CH}_3\text{Cl} + \text{OH}$  were investigated employing quantum chemistry methods and multichannel RRKM theory (Maryam and fahimeh, 2012). In the present paper, ab initio calculations have been performed similarly to the paper (Maryam and fahimeh, 2012) to study the two-channel reaction of  $\text{CH}_3\text{Cl}$  with OH radical and the two possible pathways for the reaction considered are:

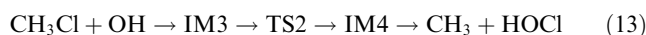
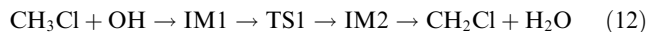


The rate constants for each reaction channel are calculated using Transition State Theory (TST) incorporating the Winger tunneling correction and the hindered rotor approximation. Furthermore, the rate constants for the dominant channel are calculated using general equation, which takes into account the rotational energy, is derived from Rice–Ramsperger–Kassel–Marcus (RRKM) theory, using the simplified version of the statistical adiabatic channel model theory and then the results have been compared with available experimental data.

## 3. Results and discussion

### 3.1. Stationary points

The optimized geometric parameters of the reactants, products, intermediates and transition states involved in  $\text{CH}_3\text{Cl} + \text{OH}$  reaction at the MP2/6-311+G (d,p) level of theory are presented in Fig. 1 along with experimental geometries (Malcolm and Chase, 1998; Malcolm et al., 1985; William et al., 1956; Escribano et al., 1996) and theoretical ones of Theodora et al. (2005). The harmonic vibrational frequencies of the intermediates and transition states are shown in Table 1 (see Table 2 in Ref. Maryam and fahimeh (2012) for reactants and products). Two channels involved in the  $\text{CH}_3\text{Cl}$  with OH reaction can be described as the following:



The major problem in the application of the unrestricted calculation is that of contamination with higher spin states. The expectation values of  $S^2$  range from 0.779 to 0.755 and from 1.00 to 0.759 before annihilation at the UMP2/6-311+G (d,p) level. After annihilation,  $S^2$  is from 0.750 to 0.750 and from 0.760 to 0.750 for the reactions (12) and (13), respectively. Therefore the spin contamination is not severe.

When the OH radical is getting closer to the hydrogen atom of the  $\text{CH}_3\text{Cl}$  molecule, the transition state TS1 is located, which connects the complex IM1 to the complex IM2 in order to form products ( $\text{CH}_2\text{Cl} + \text{H}_2\text{O}$ ) in the reaction channel (12).

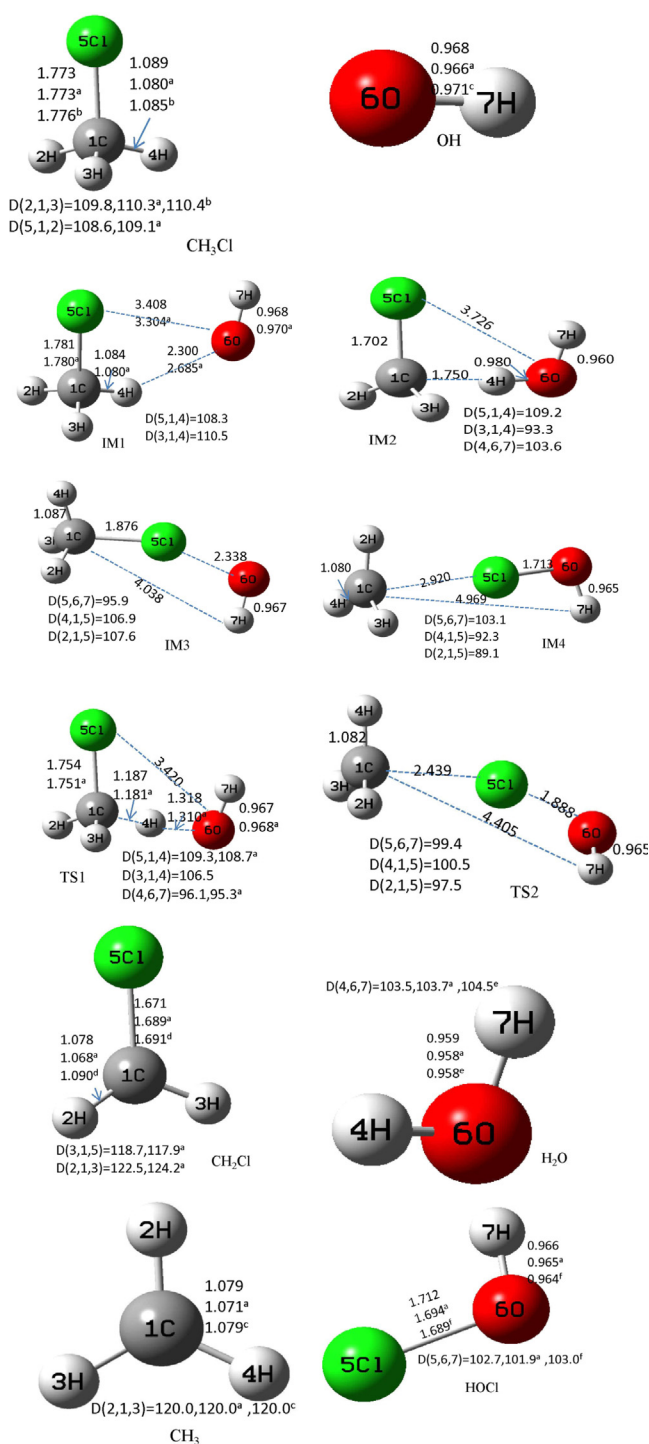


**Figure 1** Optimized geometries of all the reactants, intermediates, transition states and products for the reaction  $\text{CH}_3\text{Cl} + \text{OH}$  at the MP2/6-311+G (d,p). Bond lengths are in angstroms and angles are in degrees. <sup>a</sup>Theodora et al. (2005), <sup>b</sup>Malcolm and Chase (1998), <sup>c</sup>Malcolm et al. (1985), <sup>d</sup>Sander et al. (2002), <sup>e</sup>William et al. (1956) and <sup>f</sup>Escribano et al. (1996). (See above mentioned references for further information.)

In the reaction channel (13) a Cl atom migrates via TS2 to yield IM4 and products ( $\text{CH}_3 + \text{HOCl}$ ). In the H-abstraction reaction, as shown in Fig. 1, the O–H4 bond is shortened by

1.32 Å and it arrives to the O–H4 bond in  $\text{H}_2\text{O}$  (product) and the C–H4 bond is lengthened by 0.67 Å and in the Cl-abstraction reaction the O–Cl bond is shortened by 0.62 Å and it arrives to the O–Cl bond in  $\text{HOCl}$  (product) and the C–Cl bond is lengthened by 1.04 Å.

Table 2 shows the relative energies including zero-point energies (ZPEs) of the stationary points at different levels of theory with respect to the reactants energy. In order to obtain more reliable energies for rate constant calculation, we have used the G2MP2 method (see Table 1 in Ref. Maryam and Fahimeh (2012)).

### 3.2. Properties of the reaction path

The classical potential energy ( $V_{\text{MEP}}$ ), the ground-state vibrational adiabatic potential energy ( $V_a^G$ ) and the zero-point energy (ZPE) for reactions channels (13) as functions of the intrinsic reaction coordinates at the MP2/6-311+G (d, p) are plotted Fig. 2, where  $V_a^G(s) = V_{\text{MEP}}(s) + \text{ZPE}(s)$  (for reaction (12) see Fig. 4 in Ref Maryam and Fahimeh (2012)). Fig. 2 shows that the position of the maximum of  $V_{\text{MEP}}(s)$  is almost the same as that of  $V_a^G(s)$ , and the ZPE curve is constant in the vicinity of the saddle point. To analyze this behavior in more detail, we have presented the variations of generalized mode vibrational frequencies along the MEP for this reaction. Table 3 indicate the vibrational frequencies and the vibrational modes assignment. In Fig. 3, in the negative limit of  $s$  ( $s = -\infty$ ), the frequencies correspond to the reactants, while in the positive limit of  $s$  ( $s = +\infty$ ), the frequencies are associated with the products (see Fig. 2 in Ref Fahimeh and Maryam (2012) for reaction (12)). In Fig. 3, modes 7, 8 and 9 indicate the  $\text{CH}_3$  twist; rock in plane and rock out of plane in IM3 and it drops linearly after the saddle point and goes to zero for products, this decrease shows Cl has been added to the oxygen atom. Mode 10 represents the C–Cl stretch which their frequency increases in IM1 region and after the saddle point becomes linear. The mode shown by the solid line 11, which relates to the breaking C–Cl bond in the reactant region (the C–Cl stretch mode) and the forming Cl–O bond in the product region (the C–Cl–O stretch mode), changes sharply in the region from  $s = -1.5$ – $1.0$  ( $\text{amu}^{1/2}$  bohr) which relates to the Cl–O stretch mode. In addition, in the saddle point ( $s = 0$ ), TS2, four whole modes (rock in plane, bend in plane, rock out of plane and twist) and C–Cl–O stretch mode at 87i denote the formation of the Cl–O bond. Thus the imaginary frequency is relative to the forming bond Cl–O and breaking bond C–Cl. The two lowest frequencies (14 and 15 modes, especially 15) have a maximum near the saddle point and tend to be zero for reactants and products. These changes should cause large decreases in the ZPE (Fig. 2). These comparisons show that the reaction (13) has completely performed. The other frequencies do not change significantly in going from the reactants to products.

Comparison of modes in Table 3 shows that transition state has a reactant-like character in the reaction channel (12), it means this reaction is exothermic (Fahimeh and Maryam, 2012) and for the reaction channel (13) transition state has a product-like character, it means this reaction is endothermic. Furthermore, In order to decide whether transition states have a product- or reactant-like character, the following parameter ( $L$ ) was used (Marie-Therese et al., 1993):

**Table 1** Calculated frequencies ( $\text{cm}^{-1}$ ) of intermediates and transition states for the two reactions at the MP2/6-311 + G (d,p) level.

Species	Vibrational frequencies
IM1(C <sub>1</sub> )	24, 52, 129, 137, 164, 777, 1069, 1079, 1441, 1493, 1501, 31120, 3224, 3241, 3834 65, 93, 128, 285, 422, 763, 1051, 1060, 1407, 1515, 1517, 3138, 3236, 3238, 3761 (C <sub>s</sub> ) <sup>a</sup>
IM2(C <sub>1</sub> )	31, 661, 200, 2900, 3930, 5060, 729, 875, 1063, 1474, 1630, 3199, 3346, 3509, 3939
IM3(C <sub>1</sub> )	45, 90, 155, 283, 513, 606, 1012, 1016, 1382, 1480, 1484, 3127, 3252, 3254, 3849 <sup>b</sup>
IM4(C <sub>1</sub> )	11, 59, 61, 122, 140, 148, 557, 882, 1206, 1445, 1446, 3167, 3359, 3361, 3840
TS1(C <sub>1</sub> )	1944i, 60, 115, 265, 732, 790, 856, 1044, 1134, 1274, 1451, 1470, 3154, 3252, 3829 <sup>b</sup>
TS2(C <sub>1</sub> )	871i, 96, 169, 185, 209, 506, 561, 954, 1098, 1443, 1449, 3162, 3346, 3355, 3858 <sup>b</sup>

<sup>a</sup> Theodora et al. (2005).<sup>b</sup> Maryam and fahimeh (2012).**Table 2** Relative energies, with respect to reactant energy, of stationary points of the potential energy surface at 0 K for CH<sub>3</sub>Cl + OH reaction system calculated at different levels of theory; in kcal.mol<sup>-1</sup> (bold type shows the reaction enthalpy at 298 K).

Molecular system	G1	G2	G2MP2	G3	CBS-Q	Other works
R: CH <sub>3</sub> Cl + OH	0.00	0.00	0.00	0.00	0.00	
IM1	-1.90	-1.82	-1.84	-1.92	-1.67	
IM2	-14.51	-15.32	-15.86	-15.49	-16.45	
IM3	4.64	4.29 <sup>a</sup>	4.26 <sup>a</sup>	4.20	3.62	
IM4	27.64	27.12	26.88	26.65	26.45	
TS1	3.84	5.39 <sup>a</sup>	3.89 <sup>a</sup>	3.80	2.68	
TS2	32.03	32.00 <sup>a</sup>	32.31 <sup>a</sup>	31.45	28.97	
P: CH <sub>2</sub> Cl + H <sub>2</sub> O	-17.91	-19.10 <sup>a</sup>	-19.65 <sup>a</sup>	-19.47	-19.96	
	<b>-17.67</b>	<b>-18.86<sup>a</sup></b>	<b>-19.41</b>	<b>-19.23</b>	<b>-18.27</b>	<b>-19.43<sup>a</sup></b>
						<b>-16.61<sup>a</sup></b>
						<b>-19.47<sup>a</sup></b>
						<b>-20.62<sup>a</sup></b>
P: CH <sub>3</sub> + HOCl	27.68	27.65 <sup>a</sup>	27.45 <sup>a</sup>	27.68	27.13	
	<b>28.21</b>	<b>28.18<sup>a</sup></b>	<b>27.98<sup>a</sup></b>	<b>27.66</b>	<b>29.11</b>	<b>27.21<sup>a</sup></b>

<sup>a</sup> Maryam and fahimeh (2012).

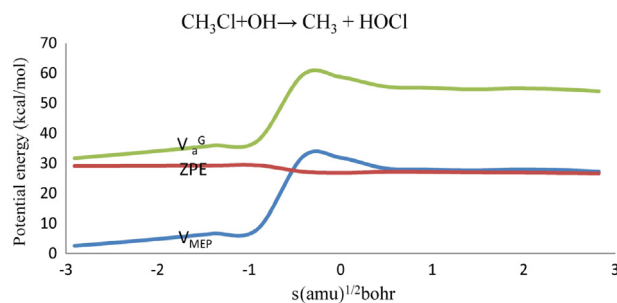
$$L = \frac{l_{\text{C1-Cl5(TS2)}} - l_{\text{C1-Cl5(CH}_3\text{Cl)}}}{l_{\text{Cl5-O6(TS2)}} - l_{\text{Cl5-O6(HOCl)}}} \quad (14)$$

when  $l_{i-j(k)}$  denotes the length of the  $i-j$  bond in the specie  $k$  (reactants, products, transition states) and where a less than unity  $L$  predicts a reactant-like character, whereas an  $L$  value greater than 1 denotes a product-like transition state. In this particular case,  $L$  is 0.27 and 3.80 for the reaction channels (12) (Fahimeh and Maryam, 2012) and (13), respectively. It means TS1 has a reactant-like character and TS2 has a product-like character.

The changes of the bond length along the MEP for the reaction CH<sub>3</sub>Cl + OH as functions of  $s$  are described in Fig. 4 for the reaction channel (13). It appears that for this reaction the active O-Cl and C-Cl bonds change strongly in the course of the reaction and the other bond lengths are almost invariant during the reaction process (see Fig. 3 in Ref Fahimeh and Maryam (2012) for reaction (15)).

### 3.3. Rate constants

For the two-channel reaction CH<sub>3</sub>Cl + OH, the individual channel rate constants,  $k_1$  and  $k_2$  are calculated using the transition state theory (Eq. (7)) incorporating the Winger tunneling correction and the hindered rotor approximation at the G2MP2 method in the temperature range of 200–2000 K.

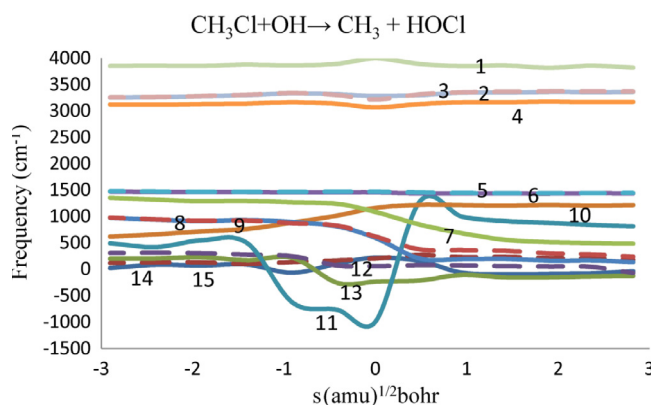
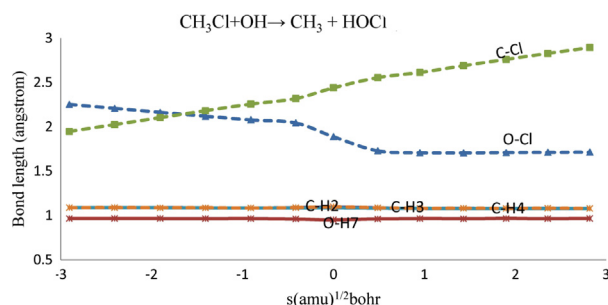
**Figure 2** Classical potential energy ( $V_{\text{MEP}}$ ), vibrational adiabatic potential energy ( $V_a^G$ ) and ZPE as functions of the intrinsic reaction coordinate,  $s$ , at the G2MP2 method for the reaction (13).

The results are given in Table 4 with experimental results (Sander et al., 2002). The total rate constant  $k_t$  for this reaction is calculated as the sum of the corresponding individual rate constants, that is,  $k_t = k_1 + k_2$ . From Tables 4 and 5 we can see that in the temperature range of 200–2000 K,  $k_1$  is larger than  $k_2$ , and the total rate constant  $k_t$  is equal to the rate constant of the H-abstraction reaction  $k_1$ , thus the H-abstraction reaction is a major reaction channel in the temperature range of 200–2000 K. Fig. 5 shows the branching fractions  $k_1/k_t$  and  $k_2/k_t$  are dependent on the temperature.

As shown in Fig. 6(a) and (b), the tunneling correction plays an important role in the lower temperature range in

**Table 3** Vibrational mode assignment the reactant region ( $s = -\infty$ ), the saddle point ( $s = 0$ ) and the product region ( $s = +\infty$ ) for the reactions (12) and (13).

Mode number	Modes assignment of $s = -\infty$ (1)	Modes assignment of $s = 0$ (1)	Modes assignment of $s = +\infty$ (1)	Modes assignment of $s = -\infty$ (2)	Modes assignment of $s = 0$ (2)	Modes assignment of $s = +\infty$ (2)
1	O-H7 stretch	O-H7 stretch	H4-O-H7 asymmetric stretch	O-H7 stretch	O-H7 stretch	O-H7 stretch
2	H2-C-H3 asymmetric stretch	H2-C-H3 asymmetric stretch	H2-C-H3 asymmetric stretch	H2-C-H3 asymmetric stretch	H2-C-H3 asymmetric stretch	H2-C-H3 asymmetric stretch
3	C-H4 stretch	C-H4-O asymmetric stretch	H4-O-H7 symmetric stretch	C-H4 stretch	CH <sub>3</sub> asymmetric stretch	CH <sub>3</sub> asymmetric stretch
4	H2-C-H3 symmetric stretch	H2-C-H3 symmetric stretch	H2-C-H3 symmetric stretch	CH <sub>3</sub> symmetric stretch	CH <sub>3</sub> symmetric stretch	CH <sub>3</sub> symmetric stretch
5	H2-C-H3 bend in plane	H2-C-H3 bend in plane	H2-C-H3 bend in plane	H2-C-H3 bend in plane	H2-C-H3 bend in plane	H2-C-H3 bend in plane
6	H3-C-H4 rock out of plane	H7-H4-CH <sub>2</sub> rock out of plane	H4-O-H7 rock out of plane	H3-C-H4 bend in plane	H2-C-H4 bend in plane	H2-C-H4 bend in plane
7	CH <sub>3</sub> bend in plane	H3-C-H4 bend in plane	H4-CH <sub>2</sub> rock in plane	CH <sub>3</sub> twist	H7-O rock in plane	H7-O rock in plane
8	CH <sub>3</sub> twist	H7-H4-CH <sub>2</sub> twist	H2-C-H3 rock out of plane	CH <sub>3</sub> rock in plane	H2-C-H3 rock out of plane	CH <sub>3</sub> bend in plane
9	CH <sub>3</sub> rock in plane	H4-CH <sub>2</sub> rock in plane	H2-C-H3 rock in plane	CH <sub>3</sub> rock out of plane	CH <sub>3</sub> rock out of plane	H7-CH <sub>2</sub> rock in plane
10	C-Cl stretch	H4-C-Cl asymmetric stretch	C-Cl stretch	C-Cl stretch	CH <sub>3</sub> twist	H7-O twist
11	H7-O twist	C-Cl stretch	H4-O-H7 rock in plane	C-Cl stretch	C-Cl-O asymmetric stretch	Cl-O stretch
12	H7-O-C bend in plane	Whole bend in plane	H <sub>2</sub> O-C bend out of plane	Whole bend in plane	Whole bend in plane	Whole bend in plane
13	H7-O bend in plane	H7-O bend in plane	H7-O bend in plane	Whole twist	Whole rock in plane	Whole rock in plane
14	H7-O-C rock in plane	Whole rock in plane	H <sub>2</sub> O-C rock in plane	Whole rock in plane	Whole rock out of plane	Whole rock in plane
15	H7-O-C twist	Whole twist	H <sub>2</sub> O-C twist	Whole bend in plane	Whole twist	Whole twist

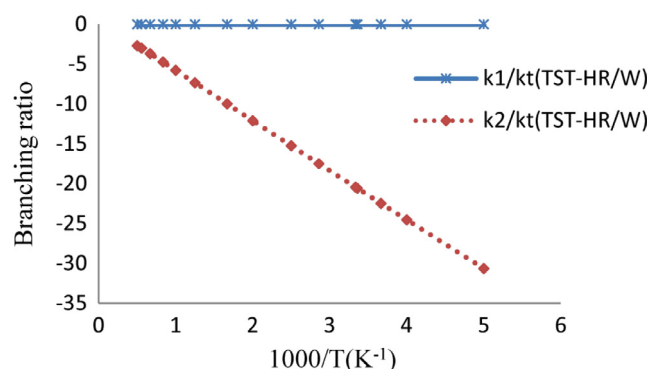
**Figure 3** Change of the generalized mode vibrational frequencies for the reaction (13) as functions of the reaction coordinate,  $s$ , at the MP2/6-311+G (d,p).**Figure 4** The changing of some key bond distances along the reaction coordinate for the reaction (13) at the MP2/6-311+G (d,p) level.

**Table 4** Calculated rate constants ( $\text{cm}^3 \text{ molecule}^{-1} \text{ s}^{-1}$ ) for the reaction (12) in the temperature range of 200–2000 K. Values in parenthesis denote power of ten.

$T$ (K)	$k_{\text{TST}}$	$k_{\text{TST}}^{\text{a}}$	$k_{\text{TST}/\text{w}}$	$k_{\text{TST}/\text{w}}^{\text{a}}$	$k_{\text{TST-HR}}$	$k_{\text{TST-HR}}^{\text{a}}$	$k_{\text{TST-HR}/\text{w}}$	$k_{\text{TST-HR}/\text{w}}^{\text{a}}$	$k_{\text{exp}}^{\text{b}}$
200	1.72(-16)	5.54(-16)	1.56(-15)	5.03(-15)	4.87(-16)	5.65(-16)	4.43(-15)	5.12(-15)	4.63(-15)
250	9.66(-16)	2.80(-15)	5.98(-15)	1.73(-14)	2.54(-15)	2.87(-15)	1.57(-14)	1.77(-14)	1.62(-14)
273	1.76(-15)	4.94(-15)	9.45(-15)	2.63(-14)	4.51(-15)	5.07(-15)	2.41(-14)	2.70(-14)	2.47(-14)
298	3.09(-15)	8.35(-15)	1.43(-14)	3.87(-14)	7.66(-15)	8.60(-15)	3.56(-14)	3.98(-14)	3.63(-14)
300	3.23(-15)	8.66(-15)	1.48(-14)	3.97(-14)	7.99(-15)	8.92(-15)	3.68(-14)	4.09(-14)	3.72(-14)
350	8.04(-15)	2.03(-14)	2.93(-14)	7.36(-14)	1.87(-14)	2.10(-14)	6.85(-14)	7.64(-14)	n/a <sup>c</sup>
400	1.66(-14)	3.98(-14)	5.03(-14)	1.20(-13)	3.68(-14)	4.16(-14)	1.11(-13)	1.26(-13)	n/a
500	5.03(-14)	1.12(-13)	1.15(-13)	2.56(-13)	1.02(-13)	1.19(-13)	2.34(-13)	2.72(-13)	n/a
600	1.15(-13)	2.43(-13)	2.20(-13)	4.61(-13)	2.17(-13)	2.63(-13)	4.13(-13)	5.00(-13)	n/a
800	3.93(-13)	7.66(-13)	5.93(-13)	1.15(-12)	6.50(-13)	8.54(-13)	9.80(-13)	1.29(-12)	n/a
1000	9.60(-13)	1.78(-12)	1.27(-12)	2.35(-12)	1.43(-12)	2.03(-12)	1.90(-12)	2.68(-12)	n/a
1200	1.93(-12)	3.46(-12)	2.36(-12)	4.23(-12)	2.65(-12)	3.99(-12)	3.25(-12)	4.89(-12)	n/a
1500	4.40(-12)	7.60(-12)	5.03(-12)	8.69(-12)	5.44(-12)	8.87(-12)	6.23(-12)	1.01(-11)	n/a
1800	8.41(-12)	1.42(-11)	9.25(-12)	1.56(-11)	9.55(-12)	1.66(-11)	1.05(-11)	1.82(-11)	n/a
2000	1.21(-11)	2.02(-11)	1.31(-11)	2.18(-11)	1.30(-11)	2.35(-11)	1.41(-11)	2.54(-11)	n/a

<sup>a</sup> Theodora et al. (2005).<sup>b</sup> Sander et al. (2002).<sup>c</sup> n/a: not available.**Table 5** Calculated rate constants ( $\text{cm}^3 \text{ molecule}^{-1} \text{ s}^{-1}$ ) for the reaction (13) in the temperature range of 200–2000 K. Values in parenthesis denote power of ten.

$T$ (K)	$k_{\text{TST}}$	$k_{\text{TST}/\text{w}}$	$k_{\text{TST-HR}}$	$k_{\text{TST-HR}/\text{w}}$
200	1.78(-46)	4.68(-46)	3.70(-46)	9.72(-46)
250	1.14(-39)	2.33(-39)	2.17(-39)	4.44(-39)
273	2.32(-37)	4.35(-37)	4.28(-37)	8.03(-37)
298	3.02(-35)	5.24(-35)	5.39(-35)	9.35(-35)
300	4.33(-35)	7.47(-35)	7.71(-35)	1.33(-34)
350	8.75(-32)	1.34(-31)	1.46(-31)	2.23(-31)
400	2.79(-29)	3.93(-29)	4.41(-29)	6.21(-29)
500	1.01(-25)	1.27(-25)	1.45(-25)	1.83(-25)
600	2.66(-23)	3.14(-23)	3.52(-23)	4.15(-23)
800	3.40(-20)	3.75(-20)	3.94(-20)	4.34(-20)
1000	2.89(-18)	3.07(-18)	3.01(-18)	3.21(-18)
1200	6.13(-17)	6.40(-17)	5.86(-17)	6.12(-17)
1500	1.45(-15)	1.49(-15)	1.24(-15)	1.28(-15)
1800	1.30(-14)	1.33(-14)	1.02(-14)	1.04(-14)
2000	4.05(-14)	4.12(-14)	2.88(-14)	2.92(-14)

**Figure 5** The logarithm of calculated branching ratio for the reaction  $\text{CH}_3\text{Cl} + \text{OH}$  as a function of  $10^3/T$ .

the H-abstraction reaction. The TST-HR/W rate constants for the reaction channel (12) are significantly larger than the TST rate constants in the temperature range of 200–1000 K and they are asymptotic to the TST ones at higher temperatures. For example, ratios  $k$  (TST/W) to  $k$  (TST) are 9.11, 4.65, 3.02, 1.50, 1.14 and 1.08 at 200, 298, 400, 800, 1500 and 2000 K, respectively. In addition, the  $k$  (TST-HR/TST) ratios are 2.82, 2.47, 2.21, 1.65, 1.23 and 1.07 at 200, 298, 400, 800, 1500 and 2000 K, respectively. Thus, the tunneling correction and the hindered rotor approximation to the calculation of rate of hydrogen abstraction are significant in the low temperatures, but the tunneling correction is important in the low temperatures. For the Cl-abstraction reaction, (13), the ratios  $k$  (TST/W) to  $k$  (TST) and the  $k$  (TST-HR/TST) ratios fall within 2.63–1.01 and 2.07–0.71 over the temperature range of 200–2000 K. In comparison with H-abstraction reaction, the tunneling correction is small for the Cl-abstraction reac-

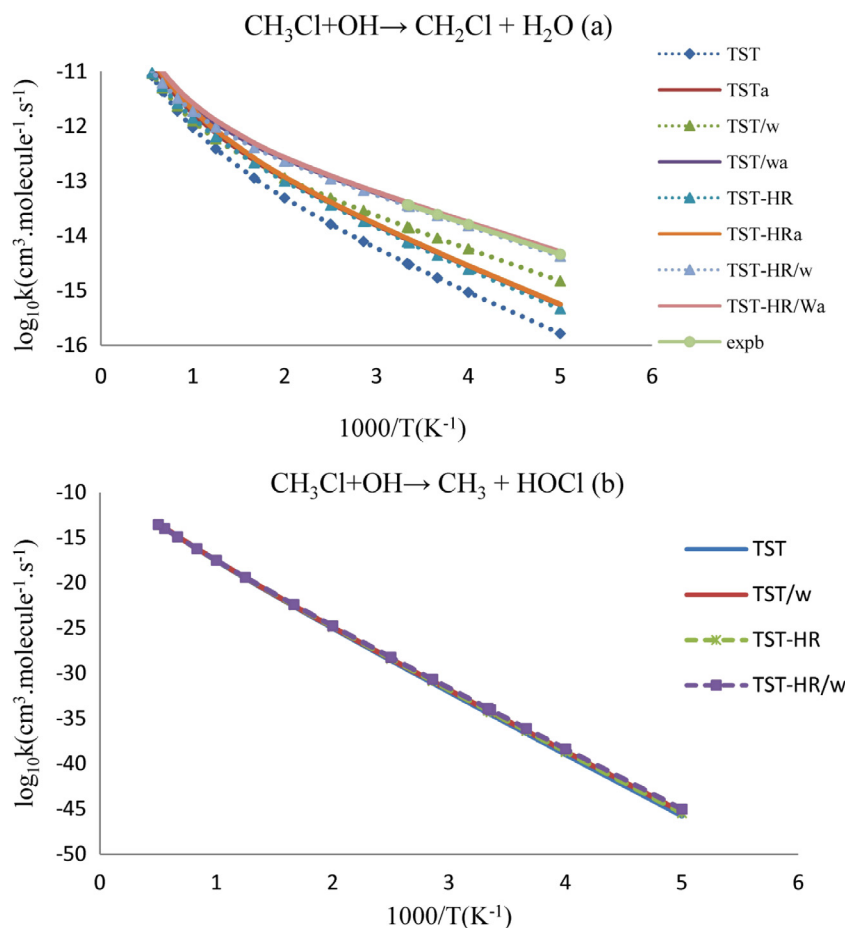


**Figure 6** (a) The logarithm of calculated rate constants as a function of  $10^3/T$  for the reaction (12). <sup>a</sup>Theodora et al. (2005) and <sup>b</sup>Sander et al. (2002). (b) Same as those in (a) except for the reaction (13).

tion. Furthermore, Fig. 6 shows that rate constants are nearly the same in the whole temperature range. Finally, the calculated rate constants for the major channel can be expressed, in  $\text{cm}^3 \text{ molecule}^{-1} \text{ s}^{-1}$ , by the following fits:

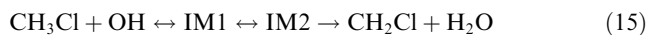
$$k = 6.91 \times 10^{-11} T^{-0.61} e^{\frac{-1290.05}{T}}$$

× for temperature range 200–400 K and

$$k = 9.11 \times 10^{-11} T^{-0.01} e^{\frac{-3576.25}{T}}$$

× for temperature range 400–2000 K.

Because the dominant channel is formation of  $\text{CH}_2\text{Cl}$  and  $\text{H}_2\text{O}$ , therefore rate constants are calculated with another method. For this channel, the reaction mechanism can be processed with the following pathway:



According to formalism of Eq (9), the rate constant for the multi-step H-abstraction from  $\text{CH}_3\text{Cl}$  by OH radical, can be calculated where  $Q_A$  and  $Q_B$  are the partition functions of  $\text{CH}_3\text{Cl}$  and OH, respectively. The bottom limit of the integral is given by the threshold energy of the reaction. The sums of states are calculated using the Beyer–Swinehart algorithm (Stephan et al., 1973; Dieter et al., 1979). Results of the rate constant calculations for the reaction under investigation are given

**Table 6** Calculated rate constants ( $\text{cm}^3 \text{ molecule}^{-1} \text{ s}^{-1}$ ) for the reactions (12) in the temperature range of 200–2000 K. Values in parenthesis denote power of ten.

$T$ (K)	$k_{\text{obs}}$	$k_{\text{TST-HR/w}}$	$k_{\text{exp}}$
200	4.50(−15)	4.43(−15)	4.63(−15)
250	1.64(−14)	1.57(−14)	1.62(−14)
273	2.55(−14)	2.41(−14)	2.47(−14)
298	3.60(−14)	3.56(−14)	3.63(−14)
300	3.74(−14)	3.68(−14)	3.72(−14)
350	5.65(−14)	6.85(−14)	n/a <sup>a</sup>
400	1.16(−13)	1.11(−13)	n/a
500	2.10(−13)	2.34(−13)	n/a
600	4.47(−13)	4.13(−13)	n/a
800	1.16(−12)	9.80(−13)	n/a
1000	1.64(−12)	1.90(−12)	n/a
1200	3.40(−12)	3.25(−12)	n/a
1500	9.21(−12)	6.23(−12)	n/a
1800	1.62(−11)	1.05(−11)	n/a
2000	1.83(−11)	1.41(−11)	n/a

<sup>a</sup> n/a: not available.

in Table 6. From Table 6, one can see that rate constants using the equations developed by Jerzy et al. are closer to the experimental results (Sander et al., 2002). The profiles obtained at

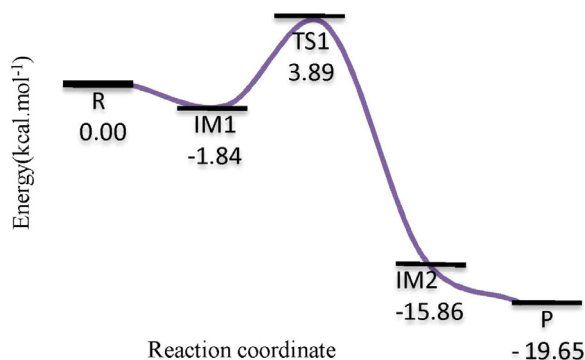


**Figure 7** Schematic energy profile of the potential energy surface for the reaction (12) at the G2MP2 level.

the G2MP2 level are displayed in Fig. 7 for this reaction. The reaction pathway is abstraction of a Hydrogen atom in the  $\text{CH}_3$  group of IM1 to produce IM2 via TS4. Attack of OH radical on  $\text{CH}_3\text{Cl}$  molecule leads, in the first elementary step, to formation of the hydrogen-bonded molecular complex IM1, and next via the transition state TS1 to the molecular complex IM2, which then dissociates into products ( $\text{CH}_2\text{Cl} + \text{H}_2\text{O}$ ). This profile shows both IM1 and IM2 complexes are located below the reactant energy level and IM1 is more unstable.

#### 4. Conclusion

In this article, the reaction  $\text{CH}_3\text{Cl} + \text{OH}$  has been studied by the ab initio direct dynamic method. Two reaction channels, in particular one H-abstraction and one Cl-abstraction, have been identified. For each individual reaction, the theoretical rate constants in the temperature range of 200–2000 K are calculated using transition state theory incorporating the Wigner tunneling correction plus the hindered rotor approximation. Theoretical results are compared to experimental data in an attempt to verify the proposed reaction mechanism. These results also indicate that, the H-abstraction is the major channel in the whole temperature range of 200–2000 K. The reaction mechanism of  $\text{CH}_3\text{Cl}$  with OH has been investigated thoroughly via the vibrational mode analysis. The vibrational mode analysis shows that the reaction mechanism is reliable.

In addition, the rate constant of the main channel has been studied by another method. This method which proceeds through formation of two loose intermediate complexes has been proposed by Jerzy et al. General equations are derived on the basis of RRKM theory and adapted by Jerzy using the simplified version of the statistical adiabatic channel model developed by Jurgen. In this approach, all the internal parameters necessary for the sum of states calculations, were determined using molecular properties, in particular, the G2MP2 energies and scaled MP2 vibrational frequencies, obtained from ab initio calculations, without any fitting or adjustable parameters. Analytical expressions obtained in this study allow the successful description of kinetics of the reactions under investigation in a wide temperature range. The results show that rate constants by this method are closer to the experimental results.

#### References

- Annia, G., Juan-Raúl, A.I., Ma, Esther, R.S., Annik, V.-B., 2002. Rate coefficient and mechanism of the gas phase OH hydrogen abstraction reaction from formic acid: A quantum mechanical approach. *J. Phys. Chem. A*, 106, 9520–9528.
- Annia, G., Juan-Raúl, A.I., Ma, Esther, R.S., Annik, V.-B., 2004. Mechanism and kinetics of the reaction of OH radicals with glyoxal and methylglyoxal: A quantum chemistry + CVT/SCT approach. *Chem. Phys. Chem.* 5 (9), 1379–1388.
- Cobos, C.J., Hippler, H., Jurgen, T., 1985. Falloff curves of the recombination reaction  $\text{O} + \text{SO} + \text{M} \rightarrow \text{SO}_2 + \text{M}$  in a variety of bath gases. *J. Phys. Chem.* 89 (9), 1778–1783.
- Dieter, C.A., Jurgen, T., Wieters, W., 1979. Unimolecular processes in vibrationally highly excited cycloheptatrienes. I. Thermal isomerization in shock waves. *J. Chem. Phys.* 70, 5107–5116.
- Escribano, R.M., Lonardo, G.Di., Fusina, L., 1996. Empirical anharmonic force field and equilibrium structure of hypochlorous acid, HOCl. *Chem. Phys. Lett.* 259, 614–618.
- Fahimeh, Sh., Maryam, D., 2012. Vibrational mode analysis for the multi-channel reaction of  $\text{CH}_3\text{O} + \text{OH}$ . *Int. J. Quantum Chem.* 112 (12), 2450–2455.
- Jerzy, T.J., Marie-Therese, R., Jean-Claude, R., Tibor, B., Sandor, D., 1998a. Theoretical study of the kinetics of the hydrogen abstraction from methanol. 1. Reaction of methanol with fluorine atoms. *J. Phys. Chem. A*, 102, 9219–9229.
- Jerzy, T.J., Marie-Therese, R., Jean-Claude, R., Tibor, B., Sandor, D., 1998b. Theoretical study of the kinetics of the hydrogen abstraction from methanol. 2. Reaction of methanol with chlorine and bromine atoms. *J. Phys. Chem. A*, 102, 9230–9243.
- Jerzy, T.J., Marie-Therese, R., Jean-Claude, R., Tibor, B., Sandor, D., 1999. Theoretical study of the kinetics of the hydrogen abstraction from methanol. 3. Reaction of methanol with hydrogen atom, methyl, and hydroxyl radicals. *J. Phys. Chem. A*, 103, 3750–3765.
- Juan-Raúl, A.I., Nelaine, M.D., Russell, J.B., Annik, V.B., 2001. On the importance of prereactive complexes in molecule–radical reactions: Hydrogen abstraction from aldehydes by OH. *J. Am. Chem. Soc.* 123, 2018–2024.
- Juan-Raúl, A.I., Armando, C.T., Annia, G., Ma, Esther, R.S., 2004. Rate coefficient and mechanism of the gas phase OH hydrogen abstraction reaction from formic acid: A quantum mechanical approach. *J. Phys. Chem. A*, 108, 2740–2749.
- Jurgen, T., 1983. Approximate expressions for the yields of unimolecular reactions with chemical and photochemical activation. *J. Phys. Chem.* 87 (10), 1800–1804.
- Jurgen, T., 1986. Elementary reactions in compressed gases and liquids: from collisional energy transfer to diffusion control. *J. Phys. Chem.* 90 (3), 357–365.
- Jurgen, T., 1994. The Polanyi Lecture. The colourful world of complex-forming bimolecular reactions. *J. Chem. Soc. Faraday Trans.* 90, 2303–2317.
- Kenneth, A.H., Michael, J.P., Struan, H.R., 1996. *Unimolecular Reactions*. John Wiley, Chichester, UK.
- Malcolm, W., Chase Jr., 1998. NIST-JANAF Thermochemical Tables, fourth ed, *J. Phys. Chem. Ref. Data. Monograph* 9.
- Malcolm, W., Chase Jr., Davies, C.A., Downey Jr., J.R., Frurip, D.J., McDonald, R.A., Syverud, A.N. 1985. Third ed. JANAF Thermochemical Tables, vol. 14, National Bureau of Standards, Washington, DC.
- Marie-Therese, R., Jean-Claude, R., Berces, T., Lendvai, G., 1993. Theoretical study of the reactions of hydroxyl radicals with substituted acetaldehydes. *J. Phys. Chem.* 97 (21), 5570–5576.
- Maryam, D., fahimeh, Sh.F., 2012. Multichannel RRKM study on the mechanisms and kinetics for the  $\text{CH}_3\text{Cl} + \text{OH}$  reaction. *Int. J. Quantum Chem.* 112 (5), 1307–1315.

- Sander, S.P., Finlayson-Pitts, B.J., Friedl, R.R., Golden, D.M., Huie, R.E., Kolb, C.E., Kurylo, M.J., Molina, M.J., Moortgat, G.K., Orkin, V.L., Ravishankara, A.R., 2002. Chemical Kinetics and Photochemical Data for Use in Atmospheric Studies, Evaluation Number 14, JPL Publication 02-25, Jet Propulsion Laboratory, Pasadena.
- Stephan, E.S., Stein, S.E., Beyer-Swinehart, R., 1973. Accurate evaluation of internal energy level sums and densities including anharmonic oscillators and hindered rotors. *J. Chem. Phys.* 58, 2438–2446.
- Theodora, D.T., Demetrios, K.P., Vasilios, S.M., 2005. An ab initio dynamics study and kinetic calculation of reaction hydrogen abstraction by OH radical from CH<sub>3</sub>Cl. *Chem. Phys.* 312, 169–176.
- Victor, H.U., Juan-Raúl, A.I., Annia, G., Isidoro, G.C., Annik, V.B., 2006. Theoretical determination of the rate constant for OH hydrogen abstraction from toluene. *J. Phys. Chem. A* 110, 10155–10162.
- William, S.B., Norman, G., Earle, K.P., 1956. Rotation-vibration spectra of deuterated water vapor. *J. Chem. Phys.* 24, 2239–2266.